# Performance of fiber-optic data links using 670-nm cw VCSELs and a monolithic Si photodetector and CMOS preamplifier

by D. M. Kuchta
H. A. Ainspan
F. J. Canora
R. P. Schneider, Jr.

**To be competitive with copper technology for links and bus applications, optoelectronics must be made affordable. One means of achieving a low-cost optoelectronics link is to adapt volume-manufactured components. This may imply CMOS optoelectronic integrated circuits (OEICs), which are suggested by the huge CMOS IC volumes being produced for computer logic and memory, and red laser diodes, which are already in demand for the consumer and storage markets. In this paper, we demonstrate a potential low-cost link using a monolithically integrated Si photodiode and CMOS preamplifier, a multimode fiber-optic transmission medium, and red, vertical-cavity surface-emitting lasers (VCSELs). The integrated receiver shows a 3.5-dB improvement in received power when light at 670 nm instead of 845 nm is used; it operates error free at both the Fibre Channel rate of 531.25 Mb/s and the SONET OC-12 rate of 622.08 Mb/s. The red VCSELs are shown to be capable of a 1.5-Gb/s transmission data rate with as little as 18 mW average power dissipation. The potential for fabricating arrays using both of these technologies for optical buses is discussed.**

©**Copyright** 1995 by International Business Machines Corporation. Copying in printed form for private use is permitted without payment of royalty provided that (1) each reproduction is done without alteration and (2) the *Journal* reference and IBM copyright notice are included on the first page. The title and abstract, but no other portions, of this paper may be copied or distributed royalty free without further permission by computer-based and other information-service systems. Permission to *republish* any other portion of this paper must be obtained from the Editor.

***0018-8646/95/$3.00 © 1995 IBM***

## Introduction

To be competitive with copper technology for links and bus applications, optoelectronics must be made affordable. One means of achieving a low-cost optoelectronics link is to adapt volume-manufactured components. This would imply CMOS optoelectronic integrated circuits, which are suggested by the huge CMOS IC volumes being produced for logic and memory applications, and red laser diodes, which are already in demand for the consumer and storage markets. Controlling packaging costs requires the use of components with fairly generous alignment tolerances, which implies a multimode fiber-optic transmission medium. In this paper, we demonstrate a potential low-cost optical fiber link using a monolithically integrated Si p-i-n photodiode and CMOS preamplifier, multimode fiber, and red vertical-cavity surface-emitting lasers (VCSELs).

There are many advantages to gain in optoelectronic links by using a monolithically integrated receiver, and there are additional advantages when the technology is CMOS. The advantages of having a monolithically integrated receiver include better immunity from electromagnetic interference (which is often picked up by the bond wire that connects the photodetector to the sensitive preamplifier), smaller size, ease in packaging (one chip instead of two), increased reliability and yield (fewer components), higher speed from reduced packaging parasitics, and ease in making arrays (one chip versus two chips and one bond wire per channel). The use of CMOS offers the additional advantages of low power consumption (especially important for arrays but dependent on the level of functionality), reasonably high speed, higher reliability (from the mature process), predictable yield (not necessarily present in the GaAs process), and photodetectors that can function from UV to near infrared.

In addition to optical links, Si integrated receivers have other potential applications such as optical clock distribution, free-space interconnections, optical storage systems, a replacement for expensive, impedance-matched coaxial connectors, and possibly even infrared wireless communication, in which a large-area detector with preamplifier could be used for lower cost and significant reduction in EMI sensitivity.

The reason for exploring the potential of red VCSELs is that these devices are currently being evaluated for use in printers and copiers and may be volume-manufactured in the form of arrays in the near future. In addition, these devices have other advantages that make them more attractive than red or infrared (CD) edge-emitting lasers and even infrared VCSELs. The red wavelength works better with shallow-junction Si p-i-n photodiodes. The red VCSEL has a much lower threshold current than edge-emitting red or near-infrared (CD) lasers. The output beam from a red VCSEL is symmetric, with a full angle of (typically) 10°, which permits efficient coupling to optical fibers. The red VCSEL has a much higher speed than red edge-emitting lasers and can easily be made into 1D and 2D arrays. The low voltage drop across a red VCSEL and its low threshold current almost make it possible to drive the device using standard 3.3-V CMOS logic levels.

For fiber-optic links there are specific discrete data rates that are used in data communication and telecommunication applications. The data communication rates set by the Fibre Channel Standard[1] start at 266 Mb/s and increase every factor of 2 to 531 Mb/s and 1062 Mb/s. The SONET standard[2] rates start at 51.840 Mb/s and increase by integer multiples to rates of 155 Mb/s, 622 Mb/s, 1244 Mb/s, and 2.488 Gb/s. Receivers and transmitters that operate up to 622 Mb/s will thus cover several of the important data and telecommunication standard transmission rates.

In the past ten years there has been some work on Si photodetectors that are compatible with CMOS and bipolar VLSI processes, and a few devices have been reported that were actually integrated with some circuitry. Yamauchi et al. [1] integrated a vertical p-i-n photodiode with polysilicon thin-film transistors. The attractive feature of this work was the ultra-low power consumption of 60 $\mu$W. The disadvantages were the speed limitation of 1 MHz and the incompatibility with CMOS processes. Recently, Wieland et al. [2] made a two-channel OEIC receiver by integrating a vertical p-i-n with a transimpedance amplifier in an 0.8-$\mu$m bipolar process with no process modifications. This circuit operated at 2.5 Gb/s, had emitter-coupled logic (ECL) output drivers, and consumed 80 mW per channel. The only drawbacks were that the 10 × 10-$\mu$m detector had a low sensitivity of 0.045 A/W, and a fairly high optical power was required to drive the output to ECL levels. The small detector size also makes it difficult to align easily with a fiber. Ghioni et al.[3] reported a lateral p-i-n photodiode compatible with Si-on-insulator (SIO) technology. This device had a small-signal bandwidth greater than 1 GHz with 5-V bias and greater than 500 MHz with 3-V bias. In addition, it had a very low dark current of 10 pA but a low sensitivity of only 0.07 A/W at 820 nm. Bassous et al. [3] fabricated a Si metal–semiconductor–metal photodetector with one modification to a bi-CMOS process. This device had a responsivity of 0.3 A/W and about 1 GHz of bandwidth at 630 nm. However, the bandwidth at 850 nm was less than 100 MHz, and the leakage currents were fairly large (≈50 nA). Chou et al. [4] also fabricated a Si metal–semiconductor–metal photodetector which had an extremely high bandwidth of 32 GHz. This high bandwidth

[1] *Fibre Channel Standard*, American National Standard for Information Systems X3T11.
[2] *Synchronous Optical Network (SONET) Transport Systems: Common Generic Criteria*, Bellcore Technical Advisory TA-NWT-00253.
[3] M. Ghioni, V. P. Kesan, and J. D. Warnock, "A High-Speed VLSI-Compatible Photodetector for Optical Interconnect Applications," unpublished work.

was achieved, however, with a 12-V bias, and the device would probably require several process modifications before it could be compatible with existing CMOS or bipolar technologies. Hartman et al. [5] integrated a vertical p-i-n photodiode with a preamplifier, postamplifier, and limiter in a Si bipolar process. This integrated receiver had a 500-MHz bandwidth, could produce ECL levels at the output with 100 $\mu$W of optical power at 820 nm, and had a great responsivity of 0.5 A/W from the vertical p-i-n, which had an anti-reflection coating. To make this integrated receiver, four extra masks and additional processing (such as a deep diffusion) were added to the bipolar process, and an extra 10-V supply was needed for the photodiode. The integrated receiver used in this paper and reported by Lim et al. [6] used a vertical p-i-n in a bi-CMOS process with no process modification or extra supply voltages. The details of this circuit are included, for completeness, in the next section.

Previous work on large-signal modulation of VCSELs has all taken place in only the last four years. Meada et al. [7] demonstrated a four-channel multiwavelength VCSEL array operating at 155 Mb/s per channel. This link used multimode fiber and an InGaAs photodiode for the 980-nm VCSELs. Choa et al. [8] showed that multi-transverse-mode VCSELs were capable of 4 Gb/s and single-mode VCSELs could be modulated to 5 Gb/s. However, no sensitivity measurement was reported, and the experiment was not fiber-based. Von Lehman et al. [9] demonstrated an 8 × 8 array of VCSELs driven to 622 Mb/s with a CMOS driver chip built to drive VCSELs. Meada et al. [10] operated a 16-channel array of 980-nm VCSELs at 5 Gb/s in a single-mode fiber link with an InGaAs p-i-n photodiode. Banwell et al. [11] combined the work of Meada et al. [7, 10] and Von Lehmen et al. [9] and analyzed an optical bus consisting of an eight-channel VCSEL transmitter with a CMOS driver chip with each channel operating at 622 Mb/s. More recently, the attention has been on large-signal modulation of multi-transverse-mode VCSELs and the application for reduced modal noise in multimode fiber links. Hahn et al. [12] showed 1-Gb/s modulation of multi-transverse-mode VCSELs in multimode fiber links and a reduction of modal noise. Kuchta and Mahon [13] also demonstrated that multi-transverse-mode 980-nm VCSELs generate very little modal noise in a multimode fiber link using an InGaAs receiver. Kuchta et al. [14] recently demonstrated 3-Gb/s operation of multi-transverse-mode VCSELs at 850 nm in a multimode fiber link and explained why high bias points are needed to obtain these higher speeds.

In the next several sections, this paper describes the details of the CMOS preamplifier with integrated photodiode, the structure, fabrication, and properties of red VCSELs, and the performance of a fiber-optic link using these two technologies for the first time.

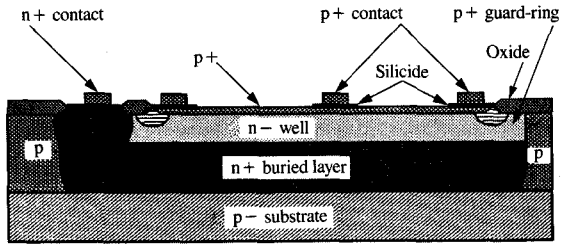


Figure 1

Cross section of the vertical p-i-n photodiode formed in the bi-CMOS process using the base and collector layers of an npn transistor.

## Integrated CMOS preamplifier and photodetector

This section describes the integrated CMOS preamplifier and integrated photodiode [6]. It is believed that this is the first time a photodiode has been successfully integrated with CMOS circuitry. This circuit and the photodiode were fabricated in a production bi-CMOS process with no process modifications [15].

The photodiode is a vertical p-i-n structure that was realized by using the base and collector layers of an npn bipolar transistor. **Figure 1** shows a cross section of the photodiode. The p+ source and drain diffusion are used to form the top electrodes and the n+ buried layer forms the bottom electrode. The n− well forms the intrinsic region of the photodiode. This region is less than 0.7 $\mu$m thick and can be fully depleted with a reverse bias of less than 2 V. The actual bias across the photodiode in the circuit is about 2.5 V when the supply is 3.3 V. The parasitic p−n+ junction below the n+ buried layer is also reverse-biased. The area of the photodiode is 75 × 75 $\mu$m and its capacitance is 1.8 pF. This area is large enough to allow about ±25 $\mu$m (1 mil) of misalignment of a 50/125-$\mu$m fiber before incurring a receiver coupling loss. The resistance of the buried layer contact is estimated to be less than 9 Ω. The responsivity of the photodiode was measured to be 0.07 A/W at a wavelength of 850 nm. This rather low responsivity is a result of using the thin layers of the bi-CMOS process without modification. At 827 nm, the absorption depth in Si is 13 $\mu$m [16], which is almost 20 times deeper than the active depth of the photodiode. At 790 nm, a typical wavelength for the "CD" laser, the absorption depth is 7.8 $\mu$m. At 650 nm, the wavelength for minimum absorption of plastic fiber, the absorption depth is 3.3 $\mu$m and the responsivity is expected to be about three times larger than at 827 nm. In shallow-junction

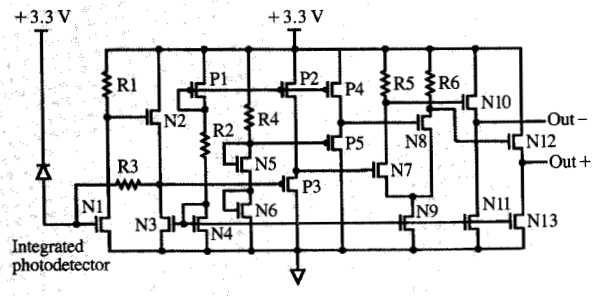


**Figure 2**

Schematic diagram of the integrated receiver.

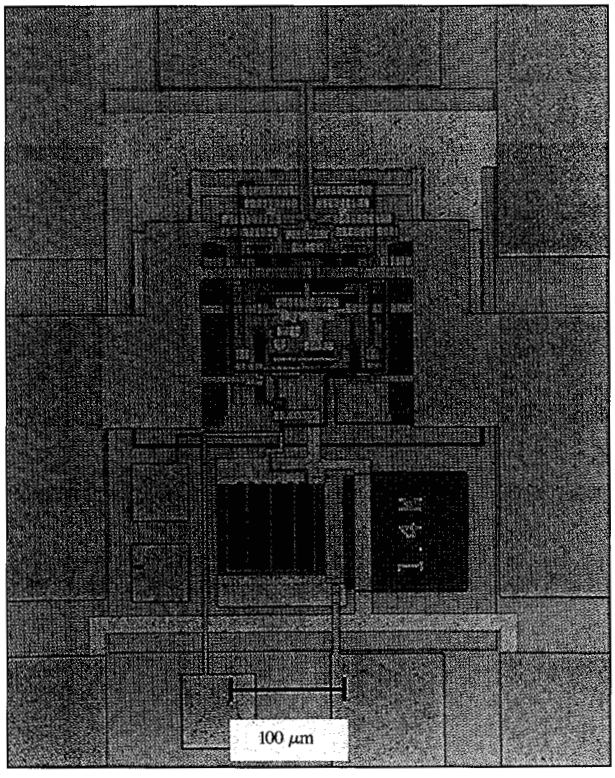


**Figure 3**

Photograph of the integrated CMOS receiver. The area including the bonding pads is 560 $\mu$m × 720 $\mu$m.

photodiodes, the light that penetrates below the junction creates electron–hole pairs, which do not experience an electric field. Consequently, these electrons either recombine locally or diffuse slowly back to the junction, where they contribute a slow tail to the photocurrent. In the current structure, there is a second reverse-biased pn junction below the photodiode junction which fortuitously collects most of the deep-generated electrons, and the slow tail effect is not observed. The small-signal bandwidth of isolated photodiodes was measured to be 700 MHz. At room temperature, the dark current is 10 nA for a 2.5-V bias.

The CMOS preamplifier is a single-ended transimpedance preamplifier which features dc input coupling. A differential output buffer stage can drive 50-Ω loads to a maximum differential peak-to-peak output level of 1 V. **Figure 2** shows the circuit schematic of the amplifier. The feedback resistor R3 has a value of 1400 Ω. However, with the additional voltage gain of the output buffer stage, the effective transimpedance of this circuit is about 3000 Ω. The open-loop gain is approximately 8, and the phase margin is 85 degrees for an input capacitance of 1.8 pF. The amplifier core dissipates 30 mW from a +3.3-V supply, with an additional 57 mW in the output source followers.

The circuit operation is as follows. The input current from the photodiode is converted to a voltage by resistor R3. The transimpedance is achieved with transistor N1 and resistor R1 to invert the signal and transistors N2/N3 to buffer the inverted signal to the opposite terminal of R3. The diode/resistor chain of R4/N5/N6 sets a voltage close to the midpoint of the voltage swing at the gate of P3. Source followers P2/P3 and P4/P5 buffer the signal and this midpoint voltage to the differential amplifier comprising N7/N8/N9 and R5/R6. N10–13 are the 50-Ω source-follower drivers. P1/R2/N4 provide internal reference voltages for biasing current sources in the circuit.

This circuit and the photodiode have been fabricated in a standard bi-CMOS process with no process modifications. This process features CMOS transistors with a minimum effective channel length of 0.45 $\mu$m. A photograph of the integrated circuit is shown in **Figure 3**. The photodetector and active circuitry occupy an area of less than 350 $\mu$m × 500 $\mu$m. This area includes a 20-pF on-chip capacitor to decouple the photodiode supply, and a p+ ring surrounding the amplifier to isolate its switching noise from the photodiode.

The circuit has been tested at the wafer level by electrical probing with optical stimulus provided by a 50-$\mu$m-core optical fiber with a rounded tip resting directly on the detector. The photodetector/preamplifier frequency response, when excited by an 850-nm-wavelength laser source (see **Figure 4**), shows a bandwidth of approximately 260 MHz for a +3.3-V supply. When the circuit is operated from a +5-V supply, the measured bandwidth increases to 300 MHz. This bandwidth is limited by the input capacitance presented by the photodetector and must be carefully optimized, since the technology and power supply determine the photodetector depletion region.

Furthermore, an active photodetector area of much less than 75 × 75 $\mu$m would require the use of special optical fiber alignment and focusing optics and would lead to higher costs, since the core diameter of a typical multimode optical fiber is 50 $\mu$m.

## Surface-emitting laser with a 670-nm vertical cavity

In this section, the structure, epitaxial growth, and properties (both ac and dc) of visible VCSELs are described. The devices used in this study were from the first wafer that produced cw (continuous-wave) lasers at room temperature [17]. It is expected that many of the properties and characteristics reported here will improve with subsequent design iterations in much the same manner as the infrared VCSELs have. Nonetheless, the performance of these early devices is quite impressive.

The red VCSEL is grown entirely by using low-pressure metalorganic vapor-phase epitaxy (MOVPE) on n+ GaAs substrates with a 6° misorientation off (100) toward $\langle 111 \rangle A$. The specific growth conditions are described in detail in [17–19]. The optical cavity is composed of a $Ga_{0.45}In_{0.55}P/(Al_{0.5}Ga_{0.5})_{0.5}In_{0.5}P$ triple-strained quantum-well active region sandwiched between $Al_{0.5}In_{0.5}P$ spacer layers. The distributed Bragg reflectors (DBR) are $AlAs/Al_{0.5}Ga_{0.5}As$, with 0.1-wave continuously parabolically graded portions inserted between the endpoint compositions to reduce resistance to current injection primarily in the p-DBR. The bottom DBR contains 55.5 periods (high-reflector, n-type Si doped to $2 \times 10^{18}$ cm$^{-3}$), and the output-coupling top DBR has 36 periods (p-type C doped to $2 \times 10^{18}$ cm$^{-3}$). The reflectivity of the top DBR is in excess of 99.9%. This results in relatively low thresholds for the lasers, at the cost of lower output power. The devices are defined by using a $H^+$ implant for current confinement. The implant is in the top p mirror and is centered just above the active region. A 10-$\mu$m-diameter current injection region is defined by this implant. The top p contact consists of a 125 × 75-$\mu$m pad with a 10-$\mu$m opening for the optical output. A mesa is defined by plasma etching around the top contact down to the active region to isolate adjacent devices.

**Figure 5** shows the light-current and the voltage-current curves for a red VCSEL with a 10-$\mu$m-diameter emitting aperture. The slope of the *V–I* curve shows a series resistance of 150 Ω between 4 and 6 mA. The two *P–I* curves are for power collected by a closely positioned large-area detector and for power coupled into a cleaved 50/125-$\mu$m graded-index multimode fiber with no coupling optics. The cleaved fiber was positioned to within 100 $\mu$m above the VCSEL. The ratio of the two power curves gives the coupling efficiency, which is slightly better than 60%. The *P–I* curve is seen to be nonlinear, a characteristic of VCSELs with emitting diameters above 10 $\mu$m. While the VCSEL cavity supports only a single longitudinal mode within the gain and mirror bandwidths, it can and does support higher-order transverse modes. The appearance of higher-order transverse modes is usually accompanied by a kink in the *P–I* curve. The other, more pronounced property of the *P–I* curve is a decrease in optical power with current beyond a certain point. This is a thermal effect, which has been attributed to a mismatch between the VCSEL cavity mode and the peak

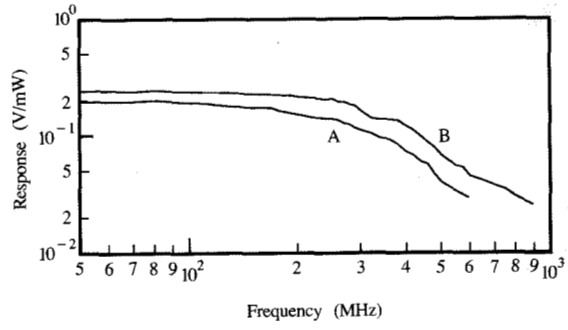


**Figure 4**

Small-signal bandwidth measurement of the integrated receiver. Curve A is for 3.3-V bias and shows a small-signal bandwidth of 260 MHz. Curve B is for a 5-V bias and shows a small-signal bandwidth of 300 MHz.

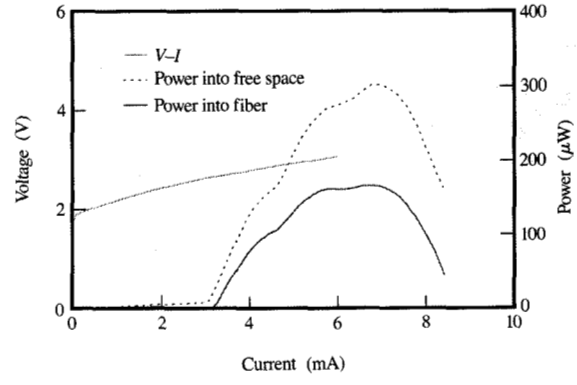


**Figure 5**

DC *V–I* and *P–I* curves for a 20-$\mu$m VCSEL. The two power curves are power into free space and power into a cleaved 50/125-$\mu$m multimode fiber, which shows a rather high coupling efficiency without special optics.

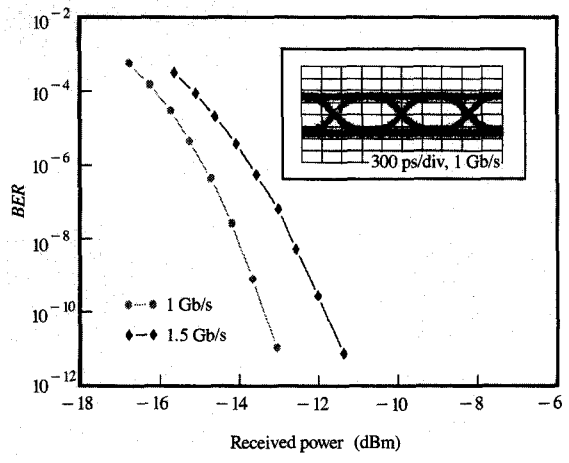


**Figure 6**

Bit-error ratio (BER) curves for a red VCSEL at 1 Gb/s and 1.5 Gb/s using a GaAs receiver with a −3-dB bandwidth of 3 GHz. The inset shows the eye diagram for the 1-Gb/s large-signal modulation.

wavelength of the gain. The point of maximum cw optical power is not the same under ac modulation. As is discussed shortly, it is possible under ac conditions to swing the current above that point to get more optical power and a larger extinction ratio. The wavelength of these devices is 670 nm and the linewidth is less than 0.1 nm while it is operating in single mode and less than 0.3 nm while it is operating in multi-transverse mode.

To assess the ultimate large-signal modulation speed of the red VCSEL, it was packaged in a very low parasitic package which consisted of a 3.5-mm high-speed coaxial connector and a submount. A 78-Ω shunt resistor was included in the package to make the entire package appear to have a 50-Ω impedance. The package was connected to a bias tee, which was used to combine the dc bias current and the ac-coupled modulation signal. The modulation signal came directly from a high-speed pattern generator. The pattern used most often was a PRBS $2^7 - 1$. A PRBS $2^{23} - 1$ pattern was also used, with no noticeable difference in performance. The PRBS $2^7 - 1$ pattern has a maximum run length of seven 1's, which is longer than the maximum run length of five 1's in the commonly used 8B/10B code [20]. To obtain maximum speed and maximum extinction ratio, the dc bias point used in large-signal modulation corresponded with the bias point of maximum cw optical power, which is 6.2 mA. The ac modulation current was adjusted for full extinction and had a peak-to-peak value of 6 mA. **Figure 6** shows a bit error ratio measurement of the red VCSEL in a short link with a GaAs receiver at data rates of 1 Gb/s and 1.5 Gb/s. The receiver bandwidth is 3 GHz. The inset shows the eye diagram at 1 Gb/s. From this one can see that the red VCSEL is fairly fast, and certainly much faster than the Si CMOS receiver. Another interesting point to note from Figure 6 is that this GaAs receiver, which at 1 Gb/s has a sensitivity of −18 dBm for a bit-error ratio (BER) = $10^{-12}$ at 850 nm, has about 5 dB less sensitivity at 670 nm. This reduced sensitivity is a result of the ten-times-larger absorption coefficient in GaAs, which means that most of the electron–hole pairs are generated within 0.3 μm of the surface, and many will recombine at the surface and thus not contribute to the photocurrent.

## Link performance and discussion

In this section, the performance of optical fiber links using the integrated CMOS preamplifier and photodiode as the receiver and the red VCSEL as the transmitter is presented and analyzed.

The red VCSEL transmitter was packaged in a low parasitic package with a 78-Ω shunt resistor, as described in the previous section. A bias tee was connected to the input of the transmitter, a current source was used to set the bias, and the pseudorandom data were ac-coupled directly from an HP70841A pattern generator. A cleaved 50/125-μm graded-index multimode fiber was positioned over the transmitter with the aide of an *XYZ* translation stage. The coupling was optimized by monitoring the coupled power with an optical power meter. The receiver was attached to a four-pin TO can package with silver epoxy. The supply pads for both the preamplifier and the photodiode were all bonded to one pin, and the grounds were all bonded to the case with the substrate. The two complementary outputs were connected to the other two pins with multiple wire bonds on each to reduce the parasitic inductance. The package was put into a socket which was soldered to a small printed circuit card having SMA connectors for the outputs and a rugged connector with a decoupling capacitor for the power supply. The outputs were ac-coupled before the SMA connectors to prevent a dc current from flowing into 50 Ω. A TE cooler/heater with a thermistor was placed in contact with the TO can for measurements as a function of temperature. To increase the received signal, both outputs were combined in a hybrid coupler to form a single-ended signal. This signal was amplified by several stages and input to an HP70842B error detector. A low-pass filter with a 900-MHz bandwidth was used to reduce the noise from the wide-bandwidth amplifiers. To determine the performance of just the transmitter and receiver together, very short links of fiber (≈10 m) were used. Later, experiments with longer lengths of fiber (up to 500 m) were employed.

The first experiment was to determine the sensitivity and the maximum transmission rate of the CMOS receiver with the red VCSEL. **Figure 7** shows bit-error ratio curves for data rates of 531.25 Mb/s (the Fibre Channel Standard half rate) and 622.08 Mb/s (the telecom SONET standard OC-12). It can be seen that the receiver sensitivity is −17.4 dBm (≈18 $\mu$W) for a BER = $10^{-10}$ at 531.25 Mb/s. It can also be seen that there is an 0.8-dB penalty in receiver sensitivity at 622.08 Mb/s, which is due to eye closure from the limited available bandwidth of 300 MHz. The inset in Figure 7 shows the eye diagram at 622.08 Mb/s.

Another set of measurements were made to check the Si-CMOS receiver sensitivity as a function of wavelength. For this, three different lasers were used: the red VCSEL at 670 nm, a commercially available CD laser at 790 nm, and an infrared VCSEL at 845 nm [21]. **Figure 8** shows the BER curves for these three wavelengths. As expected, the 670-nm curve shows the best sensitivity. There is a 3.5-dB improvement over the 845-nm source and a 2.0-dB improvement over the 790-nm source. From the data on the real and imaginary parts of the refractive index at these three wavelengths [16] and a photodiode thickness of 0.7 $\mu$m, the difference in sensitivity is expected to be 4.3 dB for 670 nm versus 827 nm and 1.8 dB for 670 nm versus 790 nm. In obtaining these numbers, it was assumed that the surface of the photodiode was not reflective. If the reflectivity of the air–silicon surface is taken into account, there is only a slight difference introduced, since the reflection coefficient changes by only 1.8% over this wavelength range. The difference between the measured improvement in sensitivity and the calculated difference is small for the two shortest wavelengths, but larger than expected, and the difference between 670 nm and 845 nm is smaller than expected. The differences can be attributed to the optical effect of the dielectric layers that cover the photodiode. These layers include polyimide, silicon nitride, and silicon dioxide. The process variation of the layer thicknesses is greater than one wavelength, which makes it difficult to predict the effect on the reflectivity of the photodiode without an accurate measurement.

To assess the receiver sensitivity as a function of temperature, the 790-nm CD laser was used as the transmitter. The data rate for these experiments was 531.25 Mb/s. The receiver was tested at 16°C and 46.8°C. These temperatures were the limits of the small TE cooler that was used. Although the receiver was powered by a voltage source, the current through the receiver changed by less than 0.2 mA over the entire temperature range. It was found that the sensitivity improved as the temperature was increased. The sensitivity at 46.8°C was 0.5 dB better than at 16°C. The measurement accuracy of the test system is 0.1 dB. If the amplifier gain can be assumed to be temperature-independent, the receiver sensitivity is

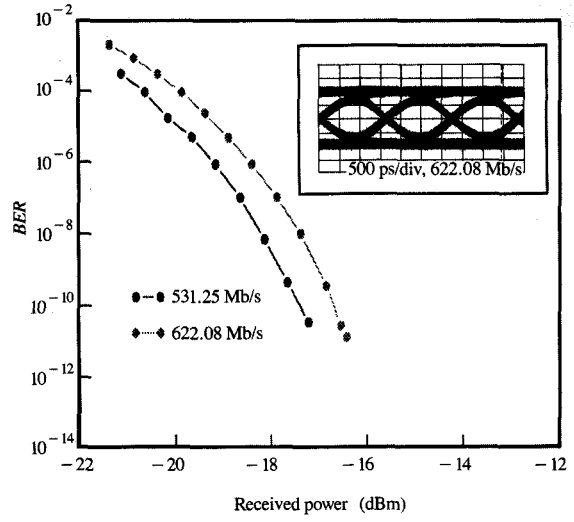


**Figure 7**

Bit-error ratio (BER) versus received optical power at 531.25 Mb/s and 622.08 Mb/s. A receiver sensitivity of −17.4 dBm ($BER = 10^{-10}$) is obtained at 531.25 Mb/s and an 0.8-dB penalty is incurred by going to 622.08 Mb/s.

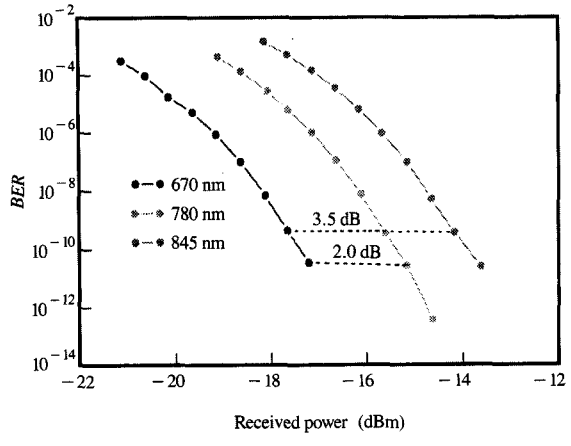


**Figure 8**

Bit-error ratio (BER) versus received optical power at 531.25 Mb/s for transmitters of three different wavelengths. The best receiver sensitivity is obtained for a wavelength of 670 nm, which is 2.0 dB better than that for 790 nm and 3.5 dB better than that for 845 nm.

expected to be worse at higher temperatures because of increases in thermal noise and photodiode leakage current. However, the output voltage swing was larger at higher temperatures, so the amplifier gain increases with temperature. Altogether, this is a rather small effect. The jitter and skew were also measured at the temperature extremes. The rms value of the jitter was 68 ps at both temperatures. The peak-to-peak jitter was 388 ps at 46.8°C and 400 ps at 16°C. Over this 30°C temperature range, the skew of the data changed by 36 ps, which is insignificant compared to the 1.8-ns bit width. The skew also had a power-dependent component for very large optical inputs which amounted to about 40 ps.

When using red VCSELs with glass fibers, it is important to know how the degradation of the fiber properties affects the link budget. The loss of glass fibers increases with decreasing wavelength because of Rayleigh scattering. This loss scales as $\lambda^{-4}$. Thus, glass fibers which typically have an attenuation of 3 dB/km at 790 nm would have 5.5 dB/km of attenuation at 670 nm. Measurements of the attenuation of 500 m of 50/125-$\mu$m graded-index fiber at 670 nm showed an insertion loss of 3 dB which included two connectors. The chromatic dispersion of the fiber will also increase from $-80$ ps/nm·km at 850 nm to $-230$ ps/nm · km for Si-doped glass fibers [22]. Even for a 1-nm source, however, the effect of chromatic dispersion on the fiber bandwidth is negligible compared to the intermodal bandwidth; since red VCSELs have a linewidth that is less than 0.3 nm, the effect of chromatic dispersion can be completely ignored. The limiting factor of the bandwidth of multimode fibers is the intermodal bandwidth. The intermodal bandwidth depends strongly on the index grading parameter $\alpha$ and the index difference between core and cladding $\Delta$ and in general is difficult to predict. It is not that difficult, however, to actually measure the intermodal bandwidth. Fiber manufacturers specify the bandwidth of multimode fibers at 850 nm and 1300 nm. For 50/125-$\mu$m graded-index multimode fiber, the bandwidth is specified as greater than 400 MHz·km for both wavelengths. For 62.5/125-$\mu$m graded-index multimode fiber, there are two classes—greater than 160 MHz·km and greater than 200 MHz·km. Research-grade fibers with bandwidths in excess of 1000 MHz·km at 850 nm can also be obtained, but at premium. The bandwidth of 500 m of 50/125-$\mu$m 1000-MHz·km (850-nm) fiber was measured to be 500 MHz·km at 670 nm. For the commercial-grade 50/125-$\mu$m fiber, the measured bandwidth was 320 MHz·km at 670 nm. For 62.5/125-$\mu$m fiber with a 200-MHz·km (850-nm) bandwidth, the measured bandwidth at 670 nm was 120 MHz·km. By using these numbers, some predictions can be made about the maximum distance for 531-Mb/s transmission using red VCSELs. For 62.5/125-$\mu$m fiber, the maximum distance is about 280 m, which is limited by the bandwidth of the fiber. For the commercial-grade 50/125-$\mu$m fiber, a distance of 750 m could be achieved, but 4 dB of fiber attenuation would be incurred. If a 3-dB fiber attenuation can be tolerated in the link budget, a link of 500 m is realistic for 50/125-$\mu$m fiber. Fibers with larger cores, in addition to their lower bandwidth, would also have an extra loss at the receiver end if coupling optics were not used. A sensitivity measurement was made using 510 m of 50/125-$\mu$m 500-MHz·km (670-nm) fiber at 531.25 Mb/s. It was found that there was no difference between the BER curves at 10 m and 510 m, although the rms jitter increased to 100 ps. One of the attractive features of the red VCSEL is that its wavelength lies within the window of low absorption of plastic fibers. Currently, plastic fibers are available in two classes: lower-loss, low-bandwidth (20 dB/km and 5 MHz·km), and high-loss, high-bandwidth (200 dB/km and 500 MHz·km). For the former plastic fiber, a link length of 20 m might be possible; for the latter plastic fiber, a link length with 3 dB of attenuation would be 15 m. Another advantage of red lasers, and especially of red VCSELs, is the reduction in modal noise that could be present in multimode fiber links. Modal noise is an additive noise that can occur in multimode fiber links when coherent sources are used as emitters and some form of loss exists in the link that is dependent on the particular fiber modes in the multimode fiber [24]. For red-VCSEL-based fiber links, a reduction of modal noise comes about both from the reduced fiber bandwidth at 670 nm and from the increase in the number of fiber modes. It has recently been shown that multi-transverse-mode VCSELs have lower coherence than single-mode VCSELs and even some types of non-self-pulsating edge-emitting lasers [12, 13], so a further reduction in modal noise is possible with multi-transverse-mode red VCSELs.

One of the biggest motivations for using integrated optoelectronics is the ease with which 1D and 2D arrays can be realized. One very important consideration for 1D arrays or optical buses is the power dissipation of each of the elements in the bus. A typical goal for a low-cost optical bus may be a 4-W power dissipation limit set by the package. If this 4 W is split evenly between the transmitter and receiver, an estimate of the size of an optical bus using red VCSELs and CMOS integrated receivers can be made. The integrated receiver consumes about 90 mW, of which only 30 mW is used by the photodiode and transimpedance amplifier. If one assumes that such a circuit would be connected to additional logic and not to a 50-$\Omega$ driver, a 30-channel optical bus would consume only 0.9 W, which leaves 1.1 W for the additional logic and control. If a 50-$\Omega$ driver is required by the application, the number of channels would have to be reduced to stay within a 2-W budget, or a package with higher heat dissipation would have to be used, which would affect the cost. The red VCSEL has a clear

advantage over edge-emitting lasers (red and CD type) with its order-of-magnitude lower current requirement. For 1-Gb/s data rates, the dc bias point of 6.2 mA corresponds to a 3-V voltage drop across the device and hence a 19-mW average power consumption. A 30-channel optical bus would consume 570 mW, which would leave 1.4 W for the driver chip (which could also be implemented in CMOS for low cost). Another consideration for optical buses is the size of the chip. As laid out (350 $\mu$m × 500 $\mu$m), a 30-channel optical bus using the Si integrated receiver would be 10.5 mm on the longest side. The area occupied by the red VCSELs is dominated by the minimum size of the bonding pad required and the need to have the bonding pad somewhat removed from the emitting area to allow space for the coupling optics. Assuming a minimum pad spacing of 250 $\mu$m center to center and a 750-$\mu$m spacing between the center of the bond pad and the emitting area, the transmitter chip would be about 7.5 mm × 1 mm. This would be roughly one fourth of the size of the driver chip. Altogether, a 30-channel bus using these technologies would occupy an area of less than 2 cm × 2 cm, consume less than 4 W, and provide a bandwidth of more than 2 GB/s over a distance of 200–300 m.

## Summary

The integrated Si receiver and red VCSELs are two promising technologies for optical data links and optical buses. The demonstrated advantages of the Si receiver are its high speed (622 Mb/s), a power sensitivity of −18 dBm for 670 nm, small size, and a low power dissipation of 30 mW (excluding 50-Ω drivers). The presumed advantages are the low cost of the chip, increased reliability, reduced packaging cost, and reduced EMI sensitivity from the monolithic design. The demonstrated advantages of the red VCSEL are its high speed (1.5 Gb/s), high fiber coupling efficiency, and low power dissipation of 18 mW. The presumed advantage of low cost hinges on its adoption by printer and copier manufacturers and on other assumptions such as wafer-level testing and screening which to date have not been demonstrated. The use of a red wavelength results in degradation of both the attenuation and bandwidth properties of multimode glass fibers. However, the properties of commercial-grade fibers at 670 nm are still sufficient for high-speed applications that require a distance of less than 300 m. Both of these technologies are quite promising for optical bus applications, which benefit greatly from monolithic array designs.

## References


1. N. Yamauchi, Y. Inaba, and M. Okamura, "An Integrated Photodetector–Amplifier Using a-Si p-i-n Photodiodes and Poly-Si Thin-Film Transistors," *IEEE Photon Technol. Lett.* **5,** No. 3, 319–321 (1993).
2. J. Wieland, H. Duran, and A. Felder, "Two-Channel 5Gbit/s Silicon Bipolar Monolithic Receiver for Parallel Optical Interconnects," *Electron. Lett.* **30,** No. 4, 358–359 (1994).
3. E. Bassous, M. Scheuermann, V. P. Kesan, M. Ritter, J. M. Halbout, and S. S. Iyer, "A High-Speed Silicon Metal–Semiconductor–Metal Photodetector Fully Integrable with (Bi)CMOS Circuits," *Proceedings of the International Electron Devices Meeting*, Washington, DC, 1991, pp. 187–190.
4. S. Y. Chou, Y. Liu, and T. F. Carruthers, "32GHz Metal–Semiconductor–Metal Photodetectors on Crystalline Silicon," *Appl. Phys. Lett.* **62,** No. 15, 1760–1762 (1992).
5. D. H. Hartman, M. K. Grace, and C. R. Ryan, "A Monolithic Silicon Photodetector/Amplifier IC for Fiber and Integrated Optics Application," *IEEE J. Lightwave Technol.* **LT-3,** No. 4, 729–738 (1985).
6. P. J. Lim, A. Y. C. Tzeng, H. L. Chuang, and S. A. St. Onge, "A 3.3 Monolithic Silicon Photodetector/CMOS Preamplifier for 531Mb/s Optical Data Link Applications," *Digest of Technical Papers, 1993 IEEE International Solid-State Circuits Conference*, San Francisco, Paper No. TA6.1, pp. 96–97 (1993).
7. M. W. Meada, C. J. Chang-Hasnain, Chinlon Lin, J. S. Patel, H. A. Johnson, and J. A. Walker, "Use of a Multiwavelength Surface-Emitting Laser Array in a Four-Channel Wavelength-Division-Multiplexed System Experiment," *IEEE Photon Technol. Lett.* **3,** 268–269 (1991).
8. F. S. Choa, Y. H. Lee, T. L. Koch, C. A. Burrus, B. Tell, J. L. Jewell, and R. E. Leibenguth, "High-Speed Modulation of Vertical-Cavity Surface-Emitting Lasers," *IEEE Photon Technol. Lett.* **3,** 697–699 (1991).
9. A. C. Von Lehmen, T. C. Banwell, R. Cordell, C. Chang-Hasnain, J. W. Mann, J. Harbison, and L. Florez, "High Speed Operation of Hybrid CMOS Vertical Cavity Surface Emitting Laser Array," *Electron. Lett.* **27,** No. 13, 1189–1191 (1991).
10. M. W. Meada, C. J. Chang-Hasnain, A. Von Lehmen, H. Izadpanah, Chinlon Lin, M. Z. Iqbal, L. Florez, and J. Harbison, "Multigigabit/s Operation of 16-Wavelength Vertical-Cavity Surface-Emitting Laser Array," *IEEE Photon Technol. Lett.* **3,** 863–865 (1991).
11. Thomas C. Banwell, Ann C. Von Lehmen, and Robert R. Cordell, "VCSE Laser Transmitters for Parallel Data Links," *IEEE J. Quantum Electron.* **29,** 635–644 (1993).
12. K. H. Hahn, M. R. Tan, Y. M. Houng, and S. Y. Wang, "Large Area Multitransverse-Mode VCSELs for Modal Noise Reduction in Multimode Fibre Systems," *Electron. Lett.* **29,** 1482–1483 (1993).
13. D. M. Kuchta and C. J. Mahon, "Mode Selective Loss Penalties in VCSEL Optical Fiber Transmission Links," *IEEE Photon Technol. Lett.* **6,** No. 2, 288–290 (1994).
14. D. M. Kuchta, R. A. Morgan, K. Kojima, M. T. Asom, G. D. Guth, M. W. Focht, and R. E. Leibenguth, "Multiple Transverse Mode VCSELs for High Speed Data Communications," *1993 IEEE Lasers and Electro-optics Society Annual Meeting Conference Proceedings*, San Jose, CA, 1993, Paper No. OC3.5, pp. 372–373.
15. B. J. Gross, H. Chuang, and T. Schmerbeck, "State-of-the-Art Analog BiCMOS," *1993 IEEE Gallium Arsenide Integrated Circuit Symposium Technical Digest*, invited paper, IEEE, Piscataway, NJ, 1993.
16. *Handbook of Optical Constants of Solids*, E. D. Palik, Ed., Academic Press Handbook Series, Orlando, FL, 1985.
17. R. P. Schneider, Jr., K. D. Choquette, J. A. Lott, K. L. Lear, J. J. Figiel, and K. J. Malloy, "Efficient Room-Temperature Continuous-Wave AlGaInP/AlGaAs Visible (670 nm) Vertical-Cavity Surface Emitting Laser Diodes," *IEEE Photon Technol. Lett.* **6,** No. 3, 313–316 (1994).
18. R. P. Schneider, Jr., E. D. Jones, J. A. Lott, and R. P. Bryan, "Photoluminescence Linewidths in Ordered and

Disordered InAlGaP Alloys Grown by Metalorganic Vapor Phase Epitaxy," *J. Appl. Phys.* **72,** 5397 (1992).
19. R. P. Schneider, Jr., R. P. Bryan, J. A. Lott, E. D. Jones, and G. R. Olbright, "MOVPE Growth of InAlGaP-Based Visible Vertical-Cavity Surface Emitting Lasers," *J. Cryst. Growth* **124,** 763 (1992).
20. A. X. Widmer and P. A. Franaszek, "A DC-Balanced, Partitioned-Block, 8B/10B Transmission Code," *IBM J. Res. Develop.* **27,** 440–451 (1983).
21. R. A. Morgan, L. M. F. Chirovsky, M. W. Focht, G. Guth, M. T. Asom, R. E. Leibenguth, K. C. Robinson, Y. H. Lee, and J. L. Jewell, "Progress in Planarized Vertical Cavity Surface Emitting Laser Devices and Arrays," *SPIE Proc.* **1562,** 149–159 (1991).
22. D. Gloge, E. A. J. Marcatili, D. Marcuse, and S. D. Personick, "Dispersion Properties of Fibers," *Optical Fiber Telecommunication*, S. E. Miller and A. G. Chynoweth, Eds., Academic Press Inc., San Diego, 1979, pp. 103–105.
23. D. Marcuse and H. M. Presby, "Fiber Bandwidth-Spectrum Studies," *Appl. Opt.* **18,** 3242–3248 (1979).
24. R. E. Epworth, "The Phenomenon of Modal Noise in Fibre Systems," *IEEE J. Quantum Electron.* **QE-18,** 543–555 (1982).

*Received June 13, 1994; accepted for publication November 20, 1994*

**Daniel M. Kuchta** *IBM Research Division, Thomas J. Watson Research Center, P.O. Box 218, Yorktown Heights, New York 10598 (KUCHTA at YKTVMV).* Dr. Kuchta received his B.S., M.S., and Ph.D. degrees in electrical engineering and computer science from the University of California at Berkeley in 1986, 1988, and 1992, respectively. He is currently a research staff member at the Thomas J. Watson Research Center, where his work and research interests include high-speed modulation of vertical-cavity surface-emitting lasers (VCSELs) and low-cost components for fiber-optic data communications.

**Herschel A. Ainspan** *IBM Research Division, Thomas J. Watson Research Center, P.O. Box 218, Yorktown Heights, New York 10598 (AINSPAN at WATSON).* Mr. Ainspan received the B.S. and M.S. degrees in electrical engineering from Columbia University, New York, in 1989 and 1991, respectively. In 1989 he joined the IBM Thomas J. Watson Research Center, where he has been involved in designing and testing of integrated circuits for high-speed optical and infrared links for computer applications, using both Si and GaAs technologies.

**Frank J. Canora** *IBM Research Division, Thomas J. Watson Research Center, P.O. Box 218, Yorktown Heights, New York 10598 (FJCJR at YKTVMV).* Mr. Canora began his career at Hypres, Inc., Elmsford, New York, as a draftsman. His work there led to an interest in integrated-circuit fabrication technology. He joined IBM at the Research Center in 1988 to work in the area of GaAs FETs. In 1991 he joined the optoelectronic packaging group to work on laser-to-fiber array packaging. He later worked on the development of low-cost optoelectronic packages. Currently Mr. Canora is involved in the design and fabrication of printed circuit boards for wireless communication links.

**Richard P. Schneider, Jr.** *Compound Semiconductor Research Laboratory, Sandia National Laboratories, Albuquerque, New Mexico 87185.* Dr. Schneider received the B.S. degree in materials science and engineering from Washington State University in 1984, and the Ph.D. degree in the same field from Northwestern University in 1989. His doctoral thesis research centered on the epitaxial growth of InAsP/InP-based strained-layer heterostructures, of interest for long-wavelength (1.3–1.55-$\mu$m) optoelectronic devices, and the optical characterization and modeling of their properties. Since 1989 Dr. Schneider has been a senior member of the technical staff in the Center for Compound Semiconductor Technologies (CCST) at Sandia National Laboratories in Albuquerque, New Mexico. His principal interests include the epitaxial design and growth of advanced semiconductor heterostructures for next-generation optoelectronic devices. He has led the effort to develop the first AlGaInP-based visible-light vertical-cavity surface-emitting laser diode, work for which he received an R&D 100 Award in 1994. The technology has matured rapidly and is now competitive with conventional AlGaAs-based IR VCSEL technology. Dr. Schneider has also been a key member of efforts at the Sandia Laboratories to further refine conventional IR VCSELs, including incorporating Al-free GaInAsP heterostructures for improved performance, and developing new approaches for ultrahigh-uniformity and high-precision epitaxial growth.